Three-Dimensional Covalent Organic Frameworks Constructed from Irregular Polyhedral Building Blocks

Jianhong Chang[†1], *Zeyue Zhang*[†2], *Haorui Zheng*[†1], *Hui Li*[*1], *Jinquan Suo*[1], *Chunqing Ji*[3], *Fenqian Chen*[1], *Valentin Valtchev*[4,5], *Shilun Qiu*[1], *Junliang Sun*[*2] *and Qianrong Fang*[*1]

[1]State Key Laboratory of Inorganic Synthesis and Preparative Chemistry, Jilin University, Changchun 130012, People's Republic of China. E-mail: qrfang@jlu.edu.cn or postlh@jlu.edu.cn

[2]College of Chemistry and Molecular Engineering, Beijing National Laboratory for Molecular Sciences, Peking University, Beijing 100871, People's Republic of China. E-mail: junliang.sun@pku.edu.cn

[3]Department of Chemical and Biomolecular Engineering, National University of Singapore, Singapore 117585

[4]Qingdao Institute of Bioenergy and Bioprocess Technology, Chinese Academy of Sciences. 189 Song Ling Rd, Qingdao, Shandong 266101, People's Republic of China

[5]Normandie Univ, ENSICAEN, UNICAEN, CNRS, Laboratoire Catalyse et Spectrochimie, 14050 Caen, France

[†]These authors contributed equally to this work

Abstract: Developing three-dimensional (3D) covalent organic frameworks (COFs) has paramount significance across numerous applications. However, the conventional design approach that relies on regular building blocks significantly restricts the structural diversity of COFs. In this study, we successfully designed and synthesized two 3D COFs, named JUC-643 and JUC-644, employing a novel strategy based on irregular 8-connected (8-c) building blocks. By using a continuous rotation electron diffraction technique combined with powder X-ray diffraction patterns, their structures were solved and revealed a unique linkage with double helical structure, a phenomenon previously unreported in COFs. In order to precisely describe the topology, these structures should be deconstructed into the unprecedented [4+3(+2)]-c nets instead of the traditional [8(+2)]-c or [6(+2)]-c net. Furthermore, one of the materials (JUC-644) has demonstrated exceptional adsorption capability towards C_3H_8 and *n*-C_4H_{10} (11.28 and 10.45 mmol g^{-1} at 298 K and 1 bar respectively), surpassing the adsorption performance of all known porous materials, and breakthrough experiments have also highlighted the remarkable C_3H_8/C_2H_6 and *n*-C_4H_{10}/C_2H_6 selectivity. This pioneering concept of incorporating irregular building blocks in 3D COFs introduces a promising avenue for designing intricate architectures while enhancing their potential application in the recovery of C_2H_6 from natural gas liquids.

Keyword: covalent organic frameworks; irregular building blocks; double links; structural diversity; adsorption and separation

Introduction

Covalent organic frameworks (COFs) represent a class of crystalline porous materials composed of covalently bonded organic building blocks, which assemble into two-dimensional (2D) or three-dimensional (3D) reticular structures. In the context of topological analysis, these building blocks can be likened to vertices and edges, as documented in early studies[1-5]. 2D COFs are characterized by covalent networks extending within 2D layers, resulting in a limited number of predictable and analyzable topologies that are relatively easier to investigate[6-11]. On the other hand, 3D COFs offer an extensive range of topological possibilities due to the diverse methods of connection they involve, leading to the formation of pores with varying types and sizes. The pioneering work conducted by Yaghi's research group in 2007[12] initiated the construction of 3D COFs exhibiting various topological features, a milestone that has been followed by the accomplishment of numerous successful efforts[13-16]. The distinct porous structure of 3D COFs determines their primary applications, with their respective topologies playing a crucial role in this regard.

As the topological structure of 3D COFs depends on the coordination number and geometrical symmetry of their organic building blocks, rational design of these building blocks is an effective way to create 3D COFs with a particular or novel topology. So far, traditional tetrahedral nodes have been the most prevalent choice for constructing 3D networks (Scheme 1a; see Supplementary Fig. 1 for details)[12,17,18]. The success in obtaining 3D COFs with zeolite **crb** topology (ZOF) and newfound **ljh** topology are typical cases of designing new topology via adjusting bond angles or steric hindrance of conventional building blocks composed of single organic molecules[19,20]. Another more sophisticated method to enrich the connective environment of topological vertices in COFs is to combine several building subunits into a building block. According to this method, building

blocks are created by connecting each vertex of a central planar (triangular, rectangular or square) building subunit to an outer triangular building subunit perpendicular to its plane, forming a prismatic building block in D_{nh} (n=2, 3, 4) or O_h point groups. Up till now, 6-connected (6-c) triangular prismatic building blocks and 8-connected (8-c) cubic or cuboid building blocks have been constructed in this way, forming highly connected 3D COFs with new topologies. However, these new topologies are still limited in types and relatively predictable because all of the current building blocks of COFs are based on planar polygons, regular polyhedrons or triangular prisms with relatively rigid structures and low degrees of configurational freedom (Scheme 1b, 1c and see Supplementary Fig. 1 for details). It is worth mentioning that for such COFs, new topologies are discovered mainly by adopting linkers with different configurations and simply changing building blocks with the same connective polyhedron can hardly produce new topologies. For instance, all of the reported [8(+2)]-c COFs are in **bcu** or its derived nets[21-24], and all of the reported [8+4]-c COFs are in **flu**, **scu** or **tty** topologies[25-28].

Despite the efforts of topological design, subject to the limited configurational and coordinative variety of the building blocks, the topological variety of COFs is significantly lower than that of metal-organic frameworks (MOFs), where the unique topological phenomenon never observed in COFs may appear. A typical example is that building blocks of MOFs may occasionally be connected by multiple links[29]. For instance, in **snf** and **fqr** topologies, every metal cluster is linked to the six nearest clusters by 12 or 10 linkers, which means partial or all of the clusters are "double-linked" [30-32]. In contrast, all reported COFs are synthesized via bottom-up or self-assembly strategies, a single link connects neighboring building blocks. The phenomenon of multiple links connecting adjacent building blocks has not been previously reported. Designing and combining building

blocks in various geometric configurations opens new opportunities for generation of novel 3D COFs, but still remains a great challenge.

Here, we present a novel synthetic strategy based on irregular polyhedral building blocks, resulting in two unique 3D COFs designated as JUC-643 and JUC-644 (JUC refers to Jilin University China). Their structures were determined using a combination of continuous rotation electron diffraction (cRED) technique and powder X-ray diffraction (PXRD). Remarkably, the irregular 8-c building blocks in these structures exhibit unexpected coordination of six, leading to the formation of unconventional "double links". This is the first reported occurrence of such a phenomenon in COF structures. Therefore, to describe the topology precisely, the framework should be deconstructed by splitting the 8-c building block into one 4-c vertex and four 3-c vertices, unveiling an unprecedented [4+3(+2)]-c topology denoted as **jca** (**jca** stands for Jilin University China-a) instead of the traditional [8(+2)]-c or [6(+2)]-c topology. JUC-644, in particular, demonstrates a remarkable adsorption capacity for C_3H_8 and *n*-C_4H_{10}, reaching an exceptional value of 11.28 mmol g^{-1} and 10.45 mmol g^{-1} at 298 K and 1 bar respectively, which surpasses the previous record among all known porous materials. To further explore its applicability, JUC-644 was subjected to breakthrough experiments for C_2H_6 recovery from simulated natural gas liquids (NGLs), where it exhibited excellent selectivity in terms of C_3H_8/C_2H_6 and *n*-C_4H_{10}/C_2H_6 ratios.

Results and discussion

Structural design

In contrast to conventional approaches that rely on regular building blocks, our strategy introduces irregular polyhedral building blocks by combining multiple organic subunits, wherein at least one

subunit assumes a 3D coordination environment (Scheme 1d-g). As an initial implementation of this strategy, we assemble four 3-c triangular outer subunits (C_{2v} symmetry) with a 4-c 3D regular or twisted tetrahedral central subunit (T_d or D_{2d} symmetry), resulting in an unconventional 8-c building unit with D_{2d} symmetry and high degrees of configurational flexibility. Importantly, the topologies constructed from these D_{2d} building blocks are inherently unpredictable and have likely not been reported in prior literature. In line with this concept, we design two unique building blocks, namely tetra[(3'',5''-diformylphenyl)phenyl] methane (TDFPM, Scheme 2a) and 3,3',5,5'-tetra[(3'',5''-diformylphenyl)-bimesitylene (TDFBM, Scheme 2b). In these designs, the sp^3-hybridized carbon atoms and the bimesityl groups naturally serve as regular and twisted tetrahedral central subunits respectively, while the (3',5'-diformylphenyl) groups act as triangular outer subunits. These distinctive 8-c building blocks are subsequently condensed with *p*-phenylenediamine (PDA, Scheme 2c) as a linear linker to construct two novel 3D COFs, namely JUC-643 and JUC-644 (Scheme 2d-h), possessing unique structural characteristics and topology.

Synthesis and characterization

Typically, these building blocks (PDA + TDFPM/TDFBM) were dispersed in 1,4-dioxane in the presence of acetic acid, and were then heated under different reaction conditions to build JUC-643 and JUC-644, respectively (see Section S2 for details). Scanning electron microscopy (SEM) and transmission electron microscopy (TEM) revealed the morphology of multichip for JUC-643 and cuboid for JUC-644 (Figure 1a and Supplementary Figs. 2-5). The Fourier transform infrared (FT-IR) spectra showed the appearance of new C=N stretching bands (1626 cm^{-1} for JUC-643 and 1624 cm^{-1} for JUC-644) and the disappearance of C=O (1702 cm^{-1} for TDFPM and 1706 cm^{-1} for TDFBM) and N−H (3324 cm^{-1} for PDA) stretching bands, manifesting the successful

polymerization of aldehyde and amine (Supplementary Figs. 6 and 7). In addition, the peaks at 161 ppm for JUC-643 and 158 ppm for JUC-644 in the solid-state ^{13}C cross-polarization magic-angle-spinning (CP/MAS) nuclear magnetic resonance (NMR) showed the presence of carbons from the imine groups (Supplementary Figs. 8 and 9). The thermogravimetric analysis (TGA, Supplementary Figs. 10 and 11) and powder X-ray diffraction (PXRD) patterns (Supplementary Figs. 12-15) revealed that both 3D COFs were stable under high temperatures (>400 °C) and in various organic solvents and acid/base aqueous solutions. The PXRD patterns of JUC-643 and JUC-644 indicate that a new crystalline phase has been formed (Supplementary Figs. 16 and 18).

Structural determination

According to PXRD patterns and electronic micrographs taken by SEM and TEM, JUC-644 exhibits significantly higher crystallinity than JUC-643. Therefore, the structure of JUC-644 was subjected to a detailed analysis. We used cRED technique to determine the structure of JUC-644. Sixteen individual datasets with a resolution up to 1.5 Å were collected at 99 K and the 3D reciprocal space was preliminarily reconstructed using the software *REDp*[33]. Unit cell of JUC-644 was firstly determined by cRED data (Figure 1c) and the reflection conditions were determined as: 0*kl*: *l*=2*n*; *h*0*l*: *l*=2*n*; *hk*0: *h*=2*n* from the 2D slices cut from the 3D reciprocal lattice, supporting the inference that space group should be *Pcca*. The unit cell (a = 31.669(6) Å, b = 17.376(3) Å, c = 25.285(4) Å, $\alpha = \beta = \gamma = 90°$) and space group was confirmed by Pawley Refinement of PXRD data with software *TOPAS* 5[34] with R_{wp} of 5.71% and R_p of 4.13%. The cRED datasets were then processed using *X-ray Detector Software* (*XDS*)[35] and six sets of them were merged by the python program package *edtools*[36] to improve the data completeness. Finally, we obtained a *.hkl peaks list and fractional coordinates of all non-hydrogen atoms were determined with software *SHELXT*[37]. This is the lowest

reported resolution of cRED data for successful structural determination using the *ab initio* methods. The final crystal structure model was obtained by the Rietveld refinement with *TOPAS* 5, with R_{wp} of 9.26% and R_p of 7.20% (Figure 1b and Supplementary Fig. 17, see Supplementary Tables 1-2 for details). The topological structure of JUC-644 is very characteristic with a 2-fold interpenetrated net, which will be discussed in detail below.

On the other hand, because of the relatively flexible structure of the 8-c building block TDFPM, the crystallinity of JUC-643 is not high enough to collect solvable X-ray or electron diffraction data. Since TDFPM and TDFBM are similar in structure, we infer that JUC-643 has the same topology with JUC-644. A non-interpenetrated net in space group *Pba2* (No.32) optimized by the *Material Studio*[38] software package matches well with the PXRD pattern (Supplementary Fig. 19). Pawley refinement was applied to PXRD data and showed low residual factors (R_p = 2.00%, R_{wp} = 2.90%, Supplementary Fig. 20, see Supplementary Table 3 for details). In addition, we also tried alternative structures, such as non-interpenetrated **bcu**, **dmf**, and **xux** net for JUC-643 and their simulated PXRD patterns did not match the experimental result (Supplementary Figs. 21-23, see Supplementary Tables 4-6 for details). All of the evidence above strongly confirms our inference that the structure of JUC-643 is the non-interpenetrated net with the same topology as JUC-644.

Notably, both 3D COFs displayed mesoscopic double helical structures, an extremely uncommon occurrence in COF structures[39]. The helices of JUC-643 are generated by condensation of the adjacent 8-c building blocks with two PDA linkers along *b*-axis. Two spirals are linked at the sp^3 hybridized carbon atom of the geometric center of TDFPM and they further propagate along [010] direction (Figure 2a, 2c and Supplementary Fig. 24). Similarly, the dual helices of JUC-644 are generated by the alignment of adjacent 8-c building blocks with two PDA linkers along the *b*-

axis. The two helices are connected by C-C bonds at the geometric center of the TDFBM motif and further propagate along [010] direction (Figure 2b, 2d and Supplementary Fig. 25). Both COFs are in achiral space groups because the helices appear in pairs in both structures and the whole frameworks are racemic.

As mentioned above, non-penetrated JUC-643 is in non-centrosymmetric *Pba*2 while 2-fold interpenetrated JUC-644 is in centrosymmetric *Pcca*. *Pba2* is a *translationengleiche* subgroup of *Pcca* in *mm*2 Laue group by removing the *c*-glide plane along [010] direction, which means the interpenetration of JUC-644 is completed by 180° rotation around the *a*- or *c*-axis rather than simple translation to form the center of symmetry in the structure (Figure 2e and 2f). This is similar to the interpenetration mode in the ZOF structure, in which two **crb** nets are interpenetrated by 90° rotation[19].

Topological analysis

Although the structures of both COFs have been determined, their topologies cannot be defined easily. According to traditional topological analysis methods, the whole building block in COFs is always regarded as a vertex. Under this deconstruction method, the structures are surprisingly in a [6(+2)]-c **pcu**-like topology: every 8-c building block is connected with 6 neighbors along 3 mutually orthogonal directions and there are 2 PDA linkers between neighboring building blocks along the direction parallel to the helices and 1 PDA along the other directions. This implies that adjacent building blocks are connected by multiple links, forming the double helical structure mentioned above, which is unreported in all known 3D COF structures (Scheme 1e and 1f). Keeping considering the topology as a [6(+2)]-c **pcu** net is unreasonable because the “double links” parts are

oversimplified to 1D and unable to accurately describe the porous and helical structures generated by the multiple links. This is also a subversive counter-example for the traditional topological analysis method of COFs, indicating that the entire building block cannot always be taken as a single topology vertex.

To precisely describe the topology of JUC-643 and JUC-644, we divided the 8-c building block into a 4-c vertex located in the center of the tetrahedron and four 3-c vertices in the center of the benzene ring of 3',5'-diformylphenyl group (Scheme 3a). In other words, the structure is deconstructed to a [4+3(+2)]-c net according to the position of the subunits rather than a [6(+2)]-c net according to the whole building block (Scheme 1g and 3b-d). The deconstruction process was completed using the software *Material Studio* manually and using software *ToposPro*[40] by automatically clustering, and both resulting topologies were analyzed and proven to be identical based on vertex symbols and td10 values (see Supplementary Table S7 for details). The result topology was further analyzed by program *Systre*[41], showing the highest space group symmetry of the topology is in *Pban* (No.50). The topology is different from all the contents in the *RCSR* database[42], which means it is a completely unprecedented topology.

Another intriguing aspect of the new topology is that the projection patterns along [110] and [$\bar{1}$10] directions are identical (Supplementary Fig. 26), suggesting the structure has a good chance to be related to tetragonal symmetry. The cell parameter was set to be *a*=*b* to make a tetragonal cell, and 3-c vertices' fractional coordinates were set to be *x*=*y* to make them on the diagonal of the *xOy* plane. The resulting vertex-only structure is obviously in tetragonal symmetry, but the helical edges along the *c* axis break the *C4* axis of rotation (Supplementary Fig. 27a and b). A tetragonal [4+4]-c topology in space group *P*4/*nbm* (No.125, a minimal *translationengleiche* supergroup of *Pban*) can

be accordingly defined by completing the edges along the *c* axis, which is also an unprecedented topology. The relationship between mentioned [4+4]-c and [4+3]-c topologies is similar to that between **pcu** and **cds** (Supplementary Fig. 27c and d). Deleting part of edges along specific directions would reduce the topological symmetry.

Derived topologies in 4-c structures can be defined by dividing a 4-c vertex into two 3-c vertices. For instance, **dmd**, **dmg**, **dmh**, **sur**, **tfi** and **tfk** are derived from **pts** by splitting tetragonal or square vertices along different directions. The twisted tetrahedral vertex in JUC-644 can be split into two triangular vertices defined in the center of the mesitylene ring, forming a novel [3+3]-c topology. This is the third new topology discovered in this work. The highest space group of this [3+3]-c topology is also *Pban*. In descending order of symmetry, the new-found [4+3]-c, [4+4]-c, and [3+3]-c topologies are respectively named as **jca**, **jcb** (**jcb** stands for Jilin University China-b) and **jcc** (**jcc** stands for Jilin University China-c, Scheme 3e and Supplementary Fig. 28, see Supplementary Tables 7-9 for details). Comparison of **jca**, **jcb**, and **jcc** with other similar topologies in *RCSR* database[42] is detailed in Supplementary Table 10 and Figs. 29 and 30.

The discovery of three new topologies indicates the success of our synthetic strategy. Notably, the number of vertices in **jca**, **jcb** and **jcc** topologies is not inversely proportional to their connected numbers, but is determined by the design of 8-c building blocks. This means the quantity ratio of topological vertices in COF structures can be defined manually by controlling the central and outer subunits ratio. For the D_{2d} 8-c building block itself reported in this article, more COFs in different topologies may be designed by adjusting subunits' orientation and steric hindrances, and by connecting the building blocks to linkers with various configurations and coordination numbers. Furthermore, new topologies can also be designed and discovered by altering the geometry of

central or outer subunits to tetrahedrons, pyramids, prisms or more complicated shapes. Building blocks may be even composed of multiple central subunits and different types of outer subunits, producing more possibilities for new topologies. The core requirement of this strategy is at least one subunit should be in 3D coordination environment, making the building block in irregular polyhedrons with high degrees of configurational freedom.

Porosity analysis

The nitrogen (N_2) adsorption and desorption isotherms were performed to determine the porosity of both COFs at 77 K. As illustrated in Supplementary Fig. 31 and Figure 1d, JUC-643 and JUC-644 exhibit a sharp gas uptake at low pressure ($P/P_0 < 0.1$) demonstrating their microporous nature. The inclination of isotherms in the pressure (P/P_0) range of 0.8 to 1.0 and slight desorption hysteresis for JUC-643 can be attributed to the presence of textural mesopores from the agglomeration of COF crystals. These two COFs both show microporous cavities and the measured pore sizes are 1.2 nm, 1.9 nm, and 1.5 nm along *a*, *b*, and *c* axis for JUC-643 and are 0.7 nm, 1.0 nm, and 1.0 nm along *a*, *b*, and *c* axis for JUC-644 (Supplementary Figs. 32-37). Their theoretical pore size distributions calculated by the nonlocal density functional theory (NLDFT) also revealed micropores with the pore sizes of 1.21, 1.81, and 1.43 nm for JUC-643, and 0.71 and 0.98 nm for JUC-644 along different axis (Supplementary Fig. 38 and Figure 1e), perfectly fitting on the proposed models. The pore size data provided additional support for the non-interpenetrated structure of JUC-643, establishing its topological congruence with that of JUC-644. Respectively, the Brunauer-Emmett-Teller (BET) surface area for JUC-643 and JUC-644 is 1464 $m^2 g^{-1}$ and 2771 $m^2 g^{-1}$ respectively (Supplementary Figs. 39 and 40).

Gas adsorption and separation

The novel porous structure and high surface area of JUC-644 provide promising potential for gas adsorption and separation. In this regard, we investigated the adsorption characteristics of JUC-644 towards various light hydrocarbon molecules. Single-component adsorption isotherms of C_2H_6, C_3H_8, and *n*-C_4H_{10} on JUC-644 were measured at three different temperatures: 283 K, 298 K, and 313 K (Figure 3a, 3b, and Supplementary Figs. 41-43). Our results reveal that JUC-644 exhibits higher adsorption capacities for C_2H_6, C_3H_8, and *n*-C_4H_{10} compared to JUC-643 at 298 K (4.83, 11.28, 10.45 mmol g^{-1} in JUC-644 and 1.23, 2.47, 3.32 mmol g^{-1} in JUC-643 respectively), demonstrating the highest C_3H_8 and *n*-C_4H_{10} adsorption uptake among all porous materials, surpassing values reported for C_3H_8 in BSF-1 (1.94 mmol g^{-1})[43], PAF-40-Fe (2.58 mmol g^{-1})[44], and g-C_3N_4@Zr–BPDC (8.90 mmol g^{-1}, Figure 3c and Supplementary Table 11)[45], as well as outperforming values reported for *n*-C_4H_{10} in NaX zeolite (1.56 mmol g^{-1})[46], Zn-BTM (2.01 mmol g^{-1})[47], and Zn-ZIF-8 (4.69 mmol g^{-1}, Figure 3d and Supplementary Table 12)[46]. The *n*-C_4H_{10} isotherms of JUC-644 exhibited a slightly steeper increase compared to C_3H_8, and both were considerably steeper than the C_2H_6 isotherm. This indicates that the framework affinity of JUC-644 for guest molecules follows the order of *n*-C_4H_{10} > C_3H_8 > C_2H_6.

The Clausius−Clapeyron equation[48] is utilized to calculate the isosteric heat of adsorption (Q_{st}) values for *n*-C_4H_{10}, C_3H_8, and C_2H_6 at near-zero loading, yielding values of 56, 41, and 29 kJ mol^{-1}, respectively (Figure 3e, see Supplementary Tables 13-15 for details). This outcome aligns with the observed lower uptake and more gradual isotherms for C_2H_6, indicating a high adsorption selectivity for *n*-C_4H_{10}/C_2H_6 and C_3H_8/C_2H_6. The ideal adsorbed solution theory (IAST) selectivity[49] parameter is paramount in assessing materials' adsorption and separation efficiency. Within the 0-100 kPa

range, the *n*-C_4H_{10}/C_2H_6 selectivity of JUC-644 exhibits an increasing trend, while the C_3H_8/C_2H_6 selectivity initially decreases and then increases. The maximum values of the selectivity of *n*-C_4H_{10}/C_2H_6 and C_3H_8/C_2H_6 at 100 kPa are 79.2 and 10.4, respectively (Figure 3f and Supplementary Figs. 44-52, see Supplementary Tables 16-19 for details).

Density-functional theory (DFT) calculations

In order to investigate the interaction between gas molecules and the channels, *ab initio* molecular dynamics (AIMD) simulations were carried out using the CP2K software, employing DFT as the computational method[50-51]. We initially positioned the gas molecules at the center of the channels and simulated their trajectory changes at 298.15 K. As is shown in Supplementary Fig. 53 and the GIF images in attaching files, during the process of simulation, the color of the guest molecules transitioned from blue to white, and then to red (the blue-to-white transition represents the adsorption process of gas molecules from the center of the channels to the channel walls, while the white-to-red transition represents the thermal motion trajectory of the molecules after adsorption within the channels). It can be observed that the white-to-red trajectories of C_2H_6 and C_3H_8 show clear separation, indicating weaker restrictive effects of the COF channels on these two gas molecules. The thermal motion within the channels is relatively facile for these molecules, resulting in faster diffusion. Furthermore, examining the positions of the white-to-red trajectories of C_2H_6 and C_3H_8, it is evident that the white-to-red trajectory of C_2H_6 is closer to the center of the COF channels, indicating weaker interaction between C_2H_6 and the channels, thus facilitating easier diffusion within the channels (Supplementary Fig. 53a-f). In contrast, the white-to-red trajectory of *n*-C_4H_{10} largely overlaps, and even partially overlaps with some blue trajectories, suggesting stronger restrictive effects of the COF channels on this molecule (Supplementary Fig. 53g-i).

Consequently, the thermal motion and diffusion of *n*-C_4H_{10} within the channels are relatively restricted, leading to slower diffusion.

Breakthrough experiment

The substantial disparity in adsorption capacities between C_2H_6 and longer alkanes suggests the promising potential of JUC-644 for recovering C_2H_6 from NGLs. The recovery of C_2H_6 from NGLs is a significant source of industrial C_2H_6, which is a primary raw material for C_2H_4 production[52,53]. Nevertheless, conventional cryogenic distillation and solvent absorption methods employed for gas separation are characterized by their high energy consumption and detrimental environmental impact. In light of these inherent shortcomings, adsorption separation has emerged as a promising and sustainable alternative, offering energy efficiency and environmental friendliness[54,55]. A key aspect of this approach lies in developing porous materials possessing exceptional adsorption capacity and separation selectivity[56,57]. Although MOFs have gained considerable attention in the realm of light hydrocarbon separation[58-60], their practical utilization in this context has been impeded by their relatively lower adsorption capacities for C_3H_8 and *n*-C_4H_{10} at ambient temperatures, as well as their inadequate stability under humid conditions. Addressing these limitations, JUC-644 stands out as an exceptional porous adsorbent, perfectly suited for ethane recovery from NGLs.

We initially tested the separation performance of JUC-644 in C_2H_6/C_3H_8 and C_2H_6/*n*-C_4H_{10} (1:1, Tfr: 2 mL min^{-1}) mixtures. The results revealed that in the C_2H_6/C_3H_8 mixture, the retention times for C_2H_6 and C_3H_8 were 73.8 min g^{-1} and 183.6 min g^{-1} (Figure 4a and Supplementary Figs. 54 and 55). In the C_2H_6/*n*-C_4H_{10} mixture, the retention times for C_2H_6 and *n*-C_4H_{10} were 61.9 min g^{-1} and 220.5 min g^{-1}, respectively (Figure 4b and Supplementary Figs. 56 and 57). To validate the

practical application of JUC-644 in C_2H_6 recovery from NGL, we also conducted separation tests on a $C_2H_6/C_3H_8/n\text{-}C_4H_{10}$ (46:34:20, v/v/v, Tfr: 5 mL min^{-1}) mixture at 298 K. The results demonstrated that C_2H_6 rapidly passed through JUC-644 with a retention time of 29.2 min g^{-1}, while C_3H_8 and $n\text{-}C_4H_{10}$ exhibited retention times of 73.8 min g^{-1} and 162 3 min·g^{-1}, respectively (Figure 4c and Supplementary Figs. 58 and 59). The yield of C_2H_6 (purity >99.99%) was 4.73 mmol g^{-1}. Furthermore, breakthrough experiments were performed under moist conditions (~50% relative humidity). The retention times of C_3H_8 and $n\text{-}C_4H_{10}$ remained relatively unchanged (73.1 min g^{-1} and 157.2 min g^{-1}, respectively) in the presence of water (Supplementary Figs. 60 and 61). Additionally, the performance of JUC-644 was verified through five consecutive separation cycles, demonstrating its sustained separation efficiency (Figure 4d). These results confirm that JUC-644 is a promising material for efficient and environment-friendly recovery of C_2H_6 from NGLs.

Conclusion

In conclusion, we have successfully designed and synthesized two novel 3D COFs, JUC-643 and JUC-644, by connecting two 8-c organic building blocks in D_{2d} symmetry via linear PDA linkers. Both COFs were determined using a combination of cRED technique and PXRD. The datasets with a resolution up to 1.5 Å were collected for JUC-644, which is the lowest reported resolution of cRED data for successful structural determination using the *ab initio* methods. Notably, these COFs exhibit intricate structures featuring interpenetration through 180° rotations, resulting in a center of symmetry and rare mesoscopic double helical linkages, representing a significant advancement in COF structures. To precisely describe their topologies, we develop a new strategy for topological analysis. The framework structures can be deconstructed by splitting the 8-c building block into one 4-c vertex and four 3-c vertices, and identified as an unprecedented [4+3(+2)]-c net (**jca**) instead of

the traditional [8(+2)]-c or [6(+2)]-c net. Additionally, through manual symmetry improvement to the tetragonal system, we defined a [4+4]-c topology (**jcb**) in the *P4/nbm* space group and a [3+3]-c topology (**jcc**) in the *Pban* space group, both of which are not also found in the RSCR or ToposPro database. This research reveals the complexity of COF structures and highlights the importance of cRED for accurate structural determination during COF topology analysis. Furthermore, JUC-644 exhibits exceptional adsorption capacities for C_3H_8 and *n*-C_4H_{10}, reaching 11.28 and 10.45 mmol g^{-1} at 298 K and 1 bar respectively, which surpasses the adsorption performance of all known porous materials. Breakthrough experiments also demonstrate the excellent C_3H_8/C_2H_6 and *n*-C_4H_{10}/C_2H_6 selectivity. Therefore, this new strategy for incorporating irregular building blocks in 3D COFs offers a promising path for designing complex COF structures. At the same time, the success of these materials in gas separation underscores the potential for C_2H_6 recovery from NGLs.

Methods

Synthesis of JUC-643. TDFPM (0.02 mmol, 17.0 mg) and PDA (0.08 mmol, 8.6 mg) were loaded into a Pyrex tube, 1.0 mL 1,4-dioxane and 0.1 mL of acetic acid (6 M) were added. The liquid nitrogen bath was used to freeze the Pyrex tube, which was evacuated to an interior pressure of ca. 19.0 mbar and flame-sealed, decreasing the whole by ca. 10.0 cm. The tube was placed in an oven at 100 ℃ for 3 d after the temperature increased to room temperature. The resulting precipitate was filtered and exhaustively washed with acetone 5 times. The obtained powder was immersed in anhydrous *n*-hexane, and the solvent was exchanged with fresh *n*-hexane several times. The sample was then transferred to a vacuum chamber and evacuated to 20 mTorr under 65 °C. Yield: 18.7 mg, 73.0%. Anal. Cald: C: 85.56; H: 4.58; N: 9.86; F: 5.99. Found: C: 85.98; H: 4.22; N: 9.35.

Synthesis of JUC-644. TDFBM (0.02 mmol, 15.3 mg) and PDA (0.08 mmol, 8.6 mg) were loaded into a Pyrex tube, 1.0 mL 1,4-dioxane, 0.1 mL aniline, and 0.1 mL of acetic acid (6 M) were added. The liquid nitrogen bath was used to freeze the Pyrex tube, which was evacuated to an interior pressure of ca. 19.0 mbar and flame-sealed, decreasing the length by ca. 10.0 cm. The tube was placed in an oven at 120 ℃ for 7 d after the temperature increased to room temperature. The resulting precipitate was filtered and exhaustively washed with acetone 5 times. The obtained powder was immersed in anhydrous *n*-hexane, and the solvent was exchanged with fresh *n*-hexane several times. The sample was then transferred to a vacuum chamber and evacuated to 20 mTorr under 65 ℃. Yield: 18.1 mg, 75.7%. Anal. Cald: C: 85.38; H: 3.85; N: 10.75. Found: C: 85.86; H: 3.51; N: 10.63.

Data availability. The authors declare that the data supporting the findings of this study are available within the Article and its Supplementary Information files, or from the corresponding author on reasonable request.

References

1. Cote, A. P. et al. Porous, crystalline, covalent organic frameworks. *Science.* **310,** 1166-1170 (2005).

2. El-Kaderi, H. M. et al. Designed synthesis of 3D covalent organic frameworks. *Science.* **316,** 268-272 (2007).

3. Ding, S.-Y. & Wang, W. Covalent organic frameworks (COFs): from design to applications. *Chem. Soc. Rev.* **42,** 548-568 (2013).

4. Diercks, C.S. & Yaghi, O. M. The atom, the molecule, and the covalent organic framework.

Science. **355,** (2017).

5. Guan, X.-Y., Chen, F.-Q., Fang, Q.-R. & Qiu, S.-L. Design and applications of three dimensional covalent organic frameworks. *Chem. Soc. Rev.* **49,** 1357-1384 (2020).

6. Colson, J. W. et al. Oriented 2D Covalent Organic Framework Thin Films on Single-Layer Graphene. *Science.* **332,** 228-231 (2011).

7. Feng, X., Ding, X. S. & Jiang, D.-L. Covalent organic frameworks. *Chem. Soc. Rev.* **41,** 6010-6022 (2012).

8. Huang, N., Wang, P. & Jiang, D.-L. Covalent organic frameworks: a materials platform for structural and functional designs. *Nat. Rev. Mater.* **1,** (2016).

9. Guan, X.-Y. et al. Chemically stable polyarylether-based covalent organic frameworks. *Nat. Chem.* **11**, 587–594 (2019).

10. Liu, Y.-Z. et al. A Stable Luminescent Covalent Organic Framework Nanosheet for Sensitive Molecular Recognition. *CCS Chem.* 1-13 (2022).

11. Wang, M.-C. et al. Exceptionally high charge mobility in phthalocyanine-based poly(benzimidazobenzophenanthroline)-ladder-type two-dimensional conjugated polymers. *Nat.Mater.* **22**, 880–887 (2023).

12. Kang, X. et al. Reticular Synthesis of tbo Topology Covalent Organic Frameworks. *J. Am. Chem. Soc.* **142,** 16346-16356 (2020).

13. Zhang, Y.-B. et al. Single-Crystal Structure of a Covalent Organic Framework. *J. Am. Chem. Soc.* **135,** 16336-16339 (2013).

14. Ma, Y.-X. et al. A Dynamic Three-Dimensional Covalent Organic Framework. *J. Am. Chem. Soc.* **139,** 4995-4998 (2017).

15. Gao, C., Li, J., Yin, S., Sun, J.-L. & Wang, C. Twist Building Blocks from Planar to Tetrahedral for the Synthesis of Covalent Organic Frameworks. *J. Am. Chem. Soc.* **142,** 3718-3723 (2020).

16. Guan, X.-Y., Fang, Q.-R., Yan, Y.-S. & Qiu, S.-L. Functional Regulation and Stability Engineering of Three-Dimensional Covalent Organic Frameworks. *Acc. Chem. Res.* **55,** 1912-1927 (2022).

17. Uribe-Romo, Fernando J. et al. A Crystalline Imine-Linked 3-D Porous Covalent Organic Framework. *J. Am. Chem. Soc.* **131,** 4570-4571 (2009).

18. Lin, G.-Q. et al. A Pyrene-Based, Fluorescent Three-Dimensional Covalent Organic Framework. *J. Am. Chem. Soc.* **138,** 3302-3305 (2016).

19. Liu, Y.-Z. et al. Design and Synthesis of a Zeolitic Organic Framework. *Angew. Chem. Int. Ed.* **61,** (2022).

20. Xie, Y. et al. Tuning the Topology of Three-Dimensional Covalent Organic Frameworks via Steric Control: From pts to Unprecedented Ijh. *J. Am. Chem. Soc.* **143,** 7279-7284 (2021).

21. Gong, C.-T. et al. Synthesis and Visualization of Entangled 3D Covalent Organic Frameworks with High-Valency Stereoscopic Molecular Nodes for Gas Separation. *Angew. Chem. Inter. Ed.* **61,** (2022).

22. Jin, F.-Z. et al. Bottom-Up Synthesis of 8-Connected Three-Dimensional Covalent Organic

Frameworks for Highly Efficient Ethylene/Ethane Separation. *J. Am. Chem. Soc.* **144,** 5643-5652 (2022).

23. Shan, Z. et al. 3D Covalent Organic Frameworks with Interpenetrated pcbTopology Based on 8-Connected Cubic Nodes. *J. Am. Chem. Soc.* **144,** 5728-5733 (2022).

24. Gropp, C., Ma, T.-Q., Hanikel, N. & Yaghi, O.M. Design of higher valency in covalent organic frameworks. *Science.* **370,** 424-+ (2020).

25. Jin, F.-Z. et al. Rationally Fabricating Three-Dimensional Covalent Organic Frameworks for Propyne/Propylene Separation. *J. Am. Chem. Soc.* **144,** 23081-23088 (2022).

26. Das, S. et al. Three-Dimensional Covalent Organic Framework with scu-c Topology for Drug Delivery. *ACS Appl. Mater. Interfaces.* **42,** 48045-48051 (2022).

27. Jin, F.-Z. et al. Rationally fabricating 3D porphyrinic covalent organic frameworks with scu topology as highly efficient photocatalysts. *Chem.* **8,** 3064-3080 (2022).

28. Wu, M.-M., Shan, Z., Wang, J.-J., Liu, T.-T. & Zhang, G. Three-dimensional covalent organic framework with tty topology for enhanced photocatalytic hydrogen peroxide production. *Chem. Eng. J.* **454,** 140121 (2023).

29. Mian, L. et al. Topological Analysis of Metal–Organic Frameworks with Polytopic Linkers and/or Multiple Building Units and the Minimal Transitivity Principle. *Chem. Soc. Rev.* **114,** 1343-1370 (2014).

30. Yang, S.-Y., Long, L.-S., Huang, R.-B. & Zheng, L.-S. Zn-8(SiO_4) ($C_8H_4O_4$) (6) (n): the firstborn of a metallosilicate-organic hybrid material family ($C_8H_4O_4$ = isophthalate). *Chem.*

Commun. **5,** 472-473 (2002).

31. Yang, S.-Y., et al. An exceptionally stable metal-organic framework constructed from the Zn-8(SiO_4) core. *Chem. Mater.* **14,** 3229–3231 (2002).

32. Fang, Q.-R., et al. Microporous metal-organic framework constructed from heptanuclear zinc carboxylate secondary building units. *Chem. Eur. J.* **12,** 3754-3758 (2006).

33. Wan, W. et al. Three-dimensional rotation electron diffraction: software RED for automated data collection and data processing. *J. Appl. Cryst.* **46**, 1863-1873 (2013).

34. Coelho, A.A. TOPAS and TOPAS-Academic: an optimization program integrating computer algebra and crystallographic objects written in C plus. *J. Appl. Cryst.* **51**, 210-218 (2018).

35. Kabsch, W. Integration, scaling, space-group assignment and post-refinement. *Acta. Cryst.* **D66**, 133-144 (2010).

36. Wang, B., Zou, X.-D. & Smeets, S. Automated serial rotation electron diffraction combined with cluster analysis: an efficient multi-crystal workflow for structure determination. *IUCrJ* **6**, 854-867 (2019).

37. Sheldrick, G.M. SHELXT - Integrated space-group and crystal-structure determination. *Acta. Cryst.* **A71**, 3-8 (2015).

38. *Materials Studio*, ver. 7.0; Accelrys Inc.: San Diego, CA.

39. Liu, Y.-Z. et al. Weaving of organic threads into a crystalline covalent organic framework. *Science.* **351**, 365-369 (2016).

40. Blatov, V.A., Shevchenko, A.P. & Proserpio, D.M. Applied Topological Analysis of Crystal

Structures with the Program Package ToposPro. *Cryst. Growth Des.* **14**, 3576-3586 (2014).

41. Delgado-Friedrichs, O. *Systre*.

42. O'Keeffe, M. et al. The Reticular Chemistry Structure Resource (RCSR) Database of, and Symbols for, Crystal Nets. Acc. Chem. Res. 41, 1782-1789 (2008).

43. Zhang, Y.-B. et al. A Microporous Metal-Organic Framework Supramolecularly Assembled from a Cu^{II} Dodecaborate Cluster Complex for Selective Gas Separation. *Angew. Chem. Int. Ed.* **58,** 8145 –8150 (2019).

44. Meng, S. et al. A facile approach to prepare porphyrinic porous aromatic frameworks for small hydrocarbon separation. *J. Mater. Chem. A.* **2,** 14536–14541 (2014).

45. Wang, S. et al. Propane-selective design of zirconium-based MOFs for propylene purification. *Chem. Eng. Sci.* **219,** 115604 (2020).

46. Kishida, K. et al. Recognition of 1,3-Butadiene by a Porous Coordination Polymer. *Angew. Chem. Int. Ed.* **55,** 13784 (2016).

47. Liao, P.-Q. et al. Controlling guest conformation for efficient purification of butadiene. *Science.* **356,** 1193–1196 (2017).

48. Pan, H.; Ritter, J. A.; Balbuena, P. B. Examination of the approximations used in determining the isosteric heat of adsorption from the Clausius-Clapeyron equation. *Langmuir.* **14**, 6323-6327 (1998).

49. Myers, A. L.; Prausnitz, J. M. Thermodynamics of mixed-gas adsorption. *AIChEJ*. **11**, 121-127 (1965).

50. Kuhne, T. D. et al. CP2K: An electronic structure and molecular dynamics software package - Quickstep: Efficient and accurate electronic structure calculations. *J. Chem. Phys.* **152,** 194103 (2020).

51. Grimme, S.; Bannwarth, C.; Schushkov, P. A Robust and Accurate Tight-Binding Quantum Chemical Method for Structures, Vibrational Frequencies, and Noncovalent Interactions of Large Molecular Systems Parametrized for All spd-Block Elements (Z = 1–86). *Chem. Theory Comput.* **13,** 1989–2009 (2017).

52. Li, L.-B. et al. Ethane/ethylene separation in a metal-organic framework with iron-peroxo sites. *Science.* **362,** 443-+ (2018).

53. Chen, K.-J. et al. Synergistic sorbent separation for one-step ethylene purification from a four-component mixture. *Science*. **366,** 241-+ (2019).

54. Li, B.-Y., Chrzanowski, M., Zhang, Y. M. & Ma, S. Q. Applications of metal-organic frameworks featuring multi-functional sites. *Coord. Chem. Rev.* **307,** 106-129 (2016).

55. Zhao, X. et al. Metal-Organic Frameworks for Separation. *Adv. Mater.* **30,** 1705189 (2018).

56. Bloch, E.-D. et al. Hydrocarbon Separations in a Metal-Organic Framework with Open Iron (II) Coordination Sites. *Science.* **335,** 1606-1610 (2012).

57. Yang, S.-H. et al. Supramolecular binding and separation of hydrocarbons within a functionalized porous metal-organic framework. *Nat. Chem.* **7,** 121-129 (2015).

58. Yuan, B.-Q., Wang, X., Zhou, X., Xiao, J. & Li, Z. Novel room-temperature synthesis of MIL-100(Fe) and its excellent adsorption performances for separation of light hydrocarbons. *Chem.*

Eng. J. **355,** 679-686 (2019).

59. Plonka, A.M. et al. Light Hydrocarbon Adsorption Mechanisms in Two Calcium-Based Microporous Metal Organic Frameworks. *Chem. Mater.* **28,** 1636-1646 (2016).

60. Han, G.-P. et al. Enhancing Higher Hydrocarbons Capture for Natural Gas Upgrading by Tuning van der Waals Interactions in fcu-Type Zr-MOFs. *Ind & Eng Chem Res.* **56,** 14633-14641 (2017).

Acknowledgements

This work was supported by National Key R&D Program of China (2022YFB3704900 and 2021YFF0500504), National Natural Science Foundation of China (22025504, 21621001, 22105082, U21A20285, 22125102, and 21527803), the SINOPEC Research Institute of Petroleum Processing, "111" project (BP0719036 and B17020), China Postdoctoral Science Foundation (2020TQ0118 and 2020M681034), Ministry of Science and Technology of the People's Republic of China (grant No. 2020YFA0210700), and the program for JLU Science and Technology Innovative Research Team. V.V., Q.F. and S.Q. acknowledge the collaboration in the Sino-French International Research Network "Zeolites".

Author contributions

Q.F., H.L., and J.S. were responsible for the overall project design, direction, and supervision. J.C. and H.Z. conducted the synthesis and characterization of all samples. Z.Z. and J.S. collected and analyzed the cRED data and topology structure. J.C., Z.Z., H.Z. and H.L. finalized the PXRD refinement and structure analyses. J.C., H.Z. and H.L. conducted the alkane sorption tests and breakthrough experiments. J.S. and F.C. performed DFT calculations and assisted with the TGA and FT-IR tests. C.J. assisted with the calculation of Q_{st} and IAST for alkane sorption. All authors contributed to the discussion of results and manuscript writing.

Additional information

Supplementary information is available in the online version of the paper. Reprints and permissions information is available online at www.nature.com/reprints. Correspondence and requests for materials should be addressed to H.L., J.S. and Q.F.

Competing interests

The authors declare no competing interests.

Figures and captions:

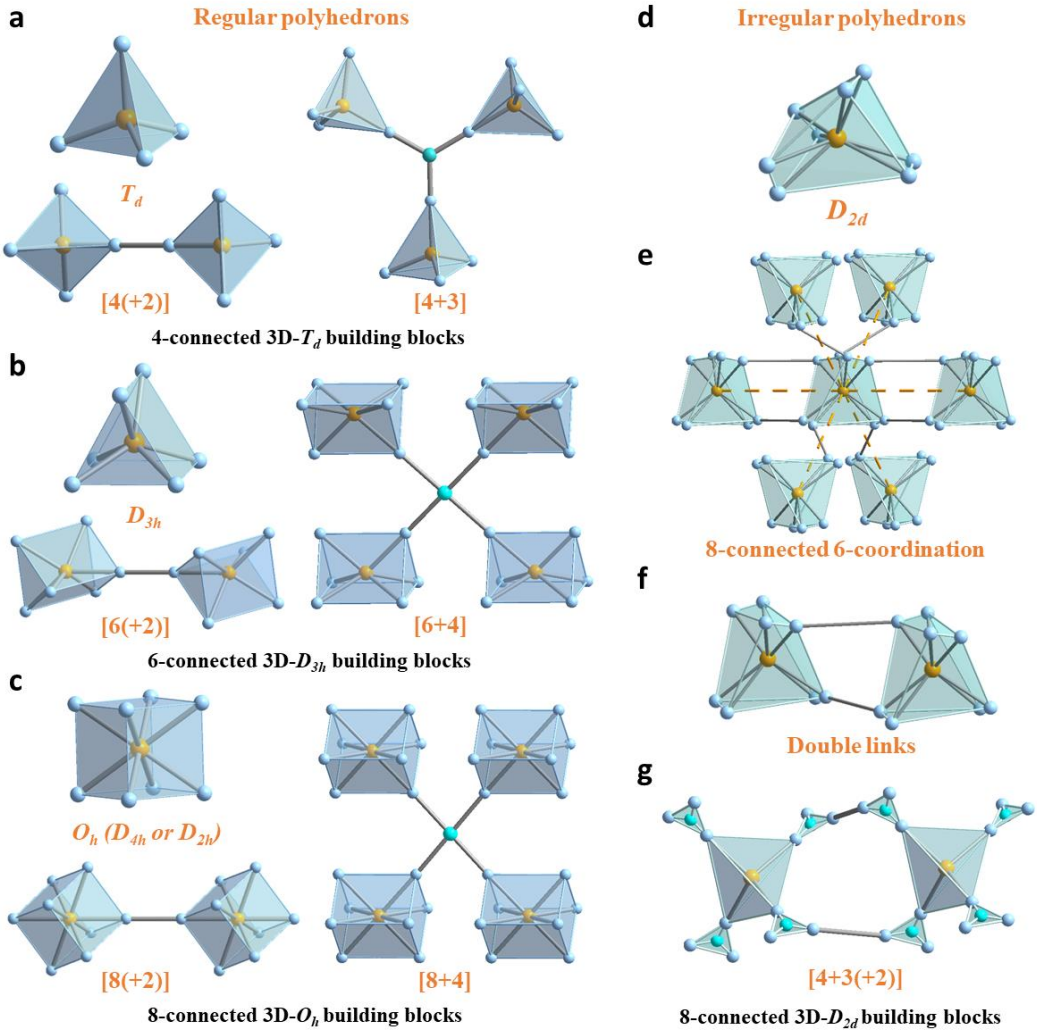

Scheme 1. Schematic illustration of 3D COFs based on different strategies. a-c, The traditional strategy based on regular polyhedrons. The [4(+2)] and [4+3] connectivity patterns using 4-connected 3D-T_d building blocks (a). The [6(+2)] and [6+4] connectivity patterns using 6-connected 3D-D_{3h} building blocks (b). The [8(+2)] and [8+4] connectivity patterns using 8-connected 3D-O_h (D_{4h}, D_{2h}) building blocks (c, and please refer to Supplementary Fig. 1 for additional connectivity patterns in 3D COFs). **d-g,** A new strategy for the design and synthesis of 3D COFs based on low-symmetry irregular polyhedrons. This strategy is exemplified by the designed and synthesized 8-connected building block with D_{2d} symmetry (d). An 8-connected 6-coordination system is

investigated in this connection, showcasing a distinctive ligand arrangement in contrast to conventional structures (e). Unique ‘‘double links’’ connectivity in the structure when considering the entire building block as a vertex (f). A remarkable [4+3(+2)] connectivity pattern when dividing the building block into a 4-c vertex and four 3-c vertices (g).

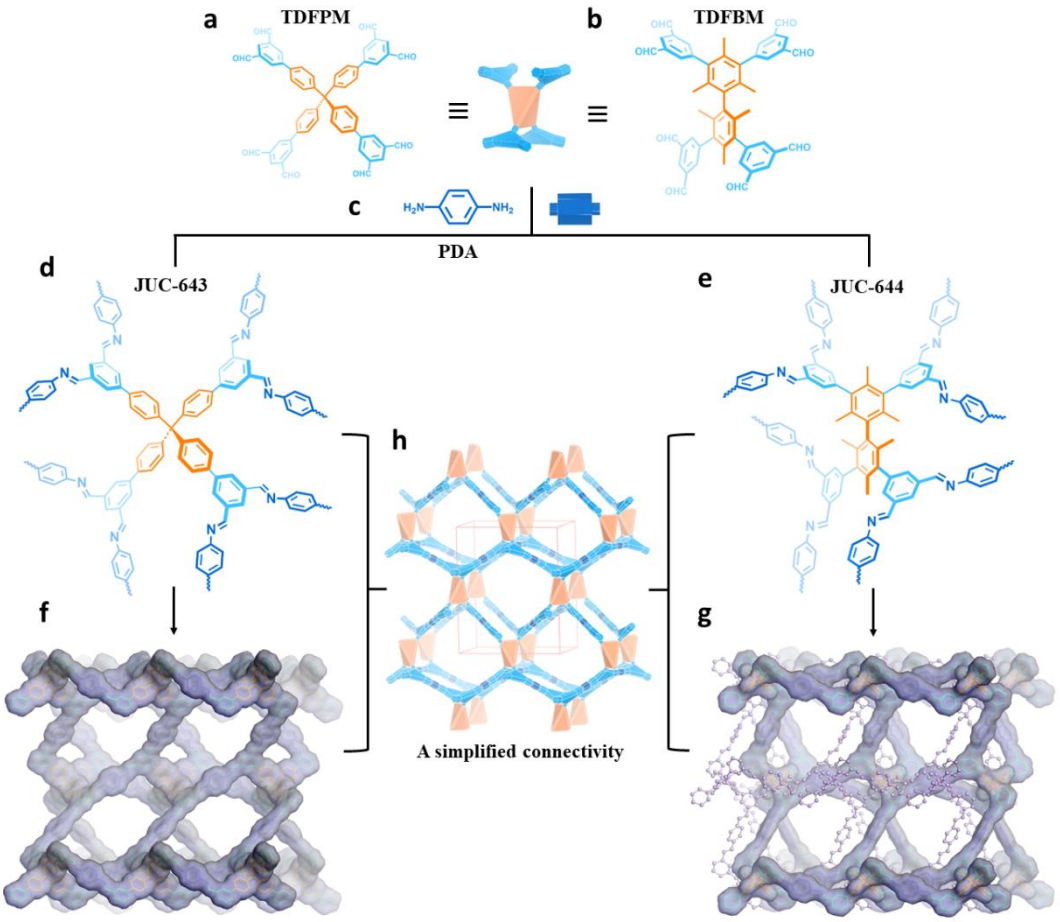

Scheme 2. Schematic Representation for constructing JUC-643 and JUC-644. a-c, Molecular structures of TDFPM and TDFBM (a and b) as 8-connected D_{2d} building blocks and PDA (c) as a linear linker. **d-g,** Two novel 3D COFs, JUC-643 (d and f) and JUC-644 (e and g), were constructed from the condensation reaction of PDA with TDFPM or TDFBM. **h,** A simplified connectivity of JUC-643 or JUC-644.

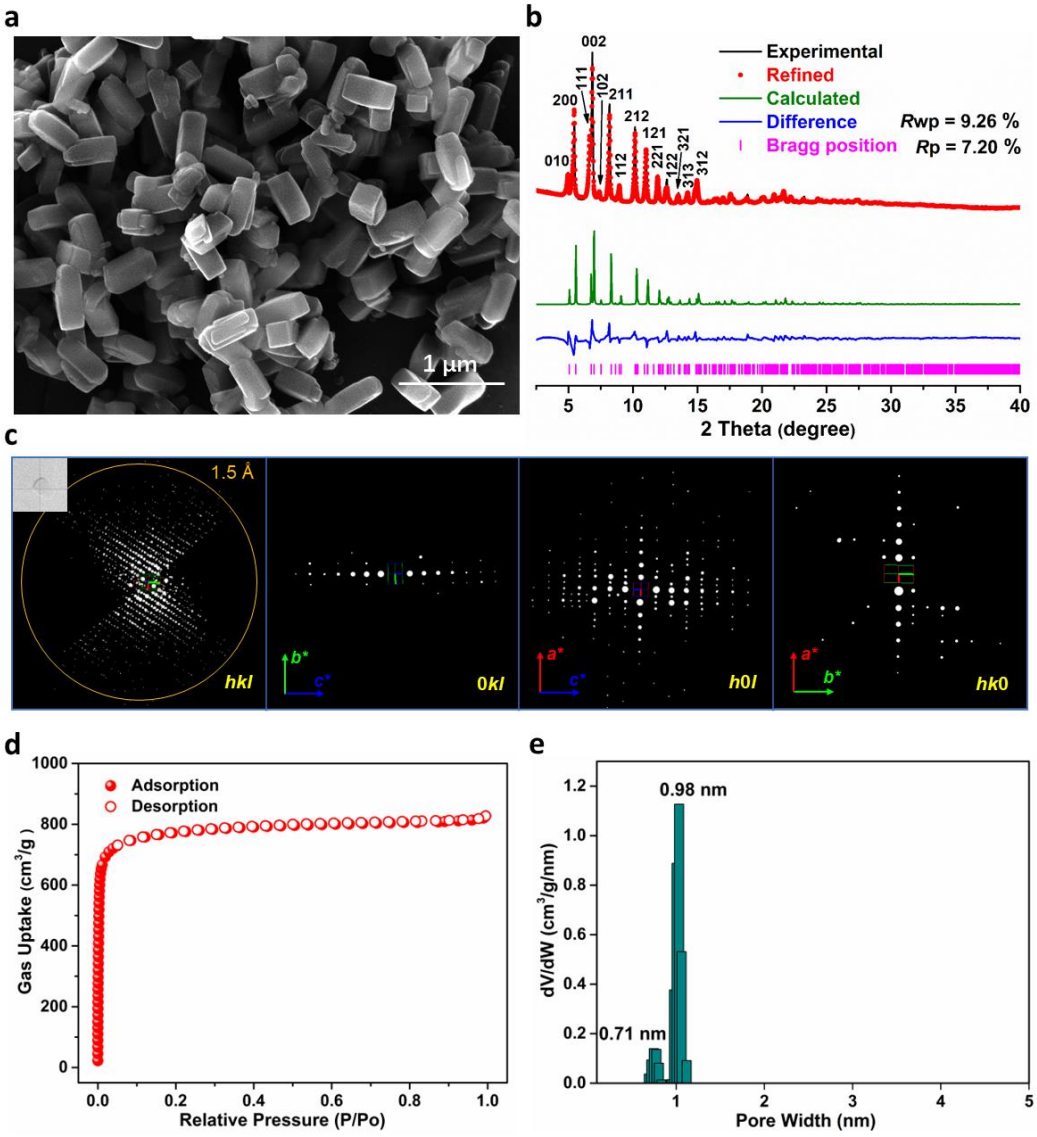

Figure 1. Structural characterization and porosity analysis of JUC-644. a-c, SEM image (a), PXRD patterns (b), and three-dimensional reciprocal lattice (c). The reflection condition can be determined as: 0*kl*: *l*=2*n*; *h*0*l*: *l*=2*n*; *hk*0: *h*=2*n*. **d,** N_2 adsorption−desorption isotherm at 77 K. **e,** Pore-size distribution calculated by fitting on the NLDFT model to the adsorption data.

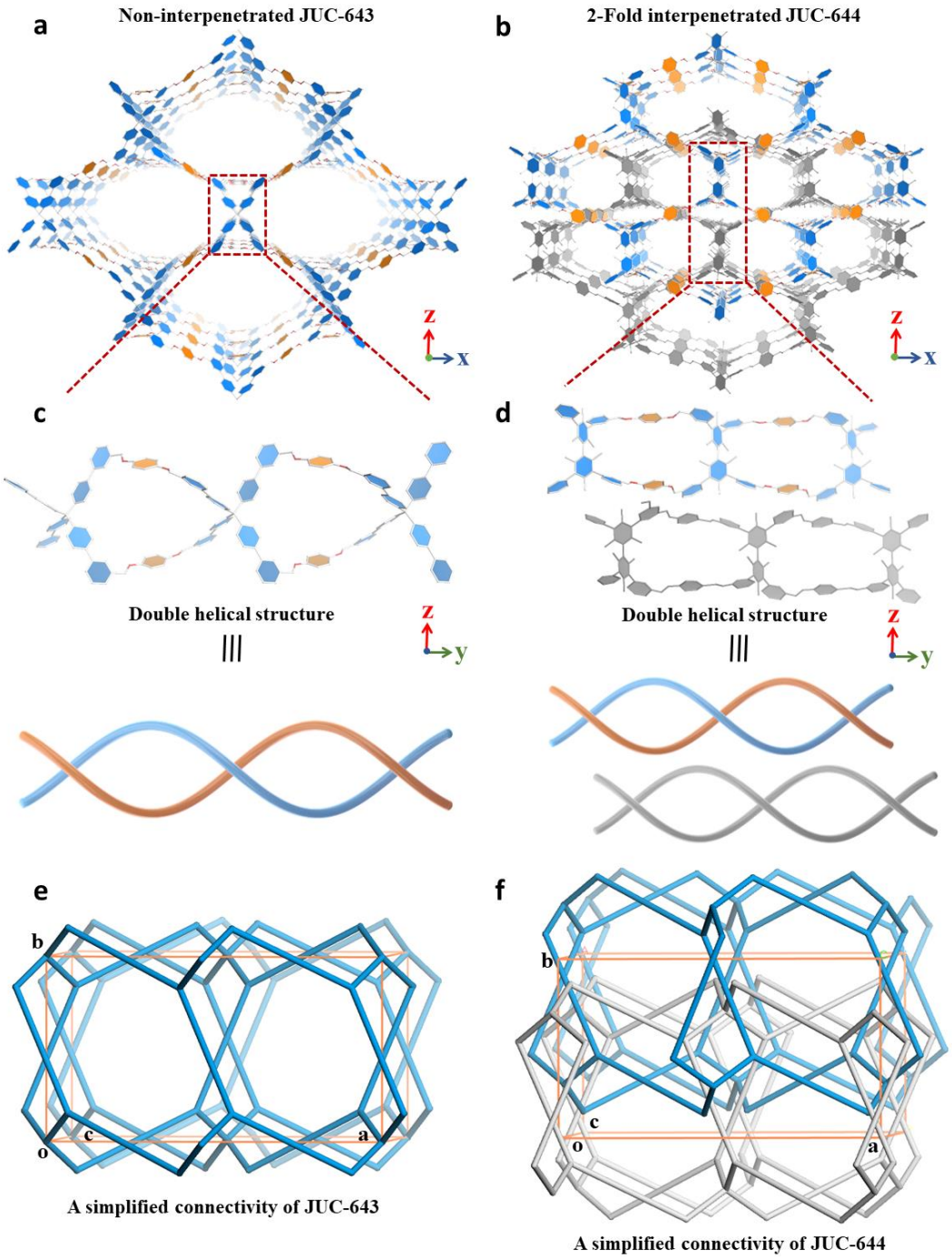

Figure 2. Structural analysis of COFs. a,b, Extended structures of non-interpenetrated JUC-643 (a) and 2-fold interpenetrated JUC-644 (b) along the *b* axis. **c,d,** Double helical structure in JUC-643 (c) and JUC-644 (d) along the *a* axis. **e,** A simplified connectivity pattern of JUC-643 in non-centrosymmetric *Pba2*. **f,** A simplified connectivity pattern of JUC-644 in centrosymmetric *Pcca*, forming a symmetric center through interpenetration.

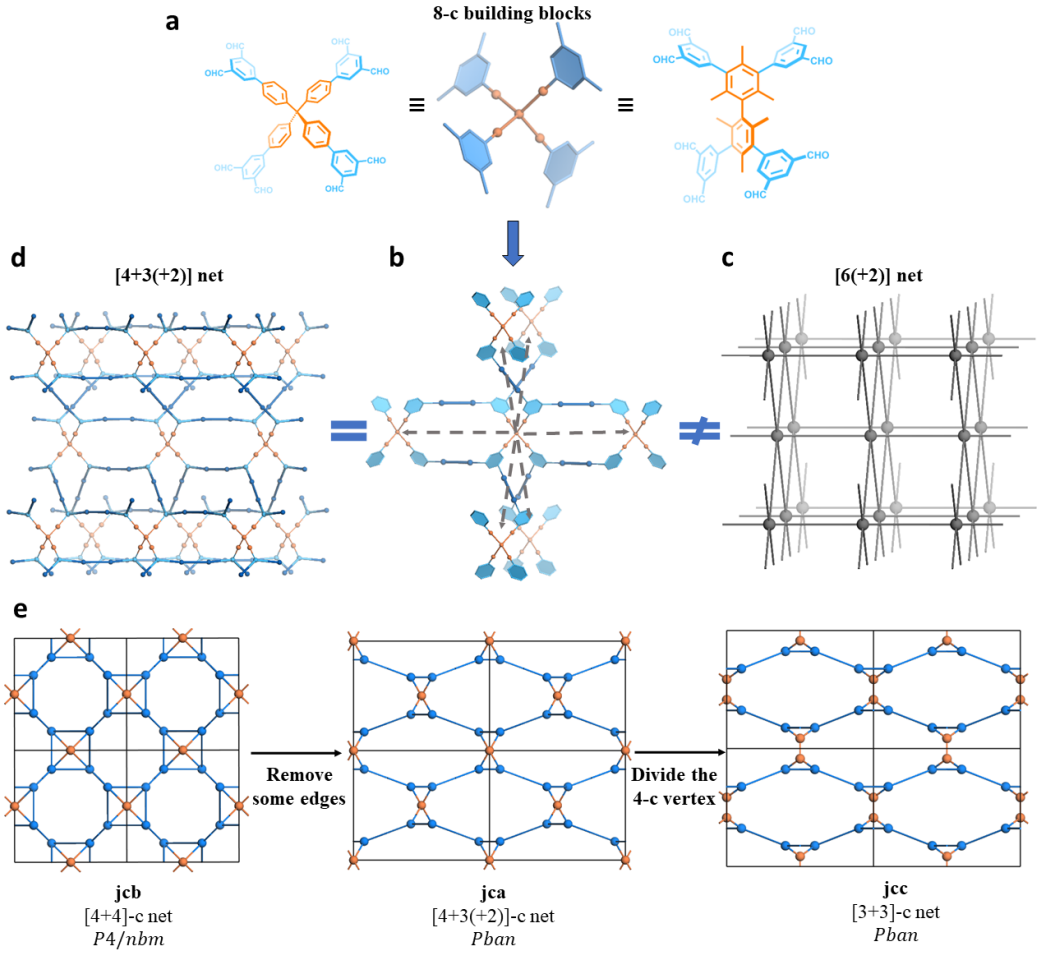

Scheme 3. Schematic illustration of the discovery of novel topologies. a,b, Simplified 8-connected building blocks (a) and COF framework with linearized double links (b). **c,** a [6(+2)]-c net based on traditional topological analysis, where the entire building block is considered as a vertex. **d,** A [4+3(+2)]-c net from the new topology analysis strategy, where the 8-c building block is divided into one 4-c vertex and four 3-c vertices for a precise topological representation. **e,** Three novel topological structures ranked in descending order of symmetry. By adjusting the symmetry and 3-c vertex coordinates, a [4+4]-c **jcb** net was discovered. Splitting the 4-c vertex revealed a [3+3]-c **jcc** net.

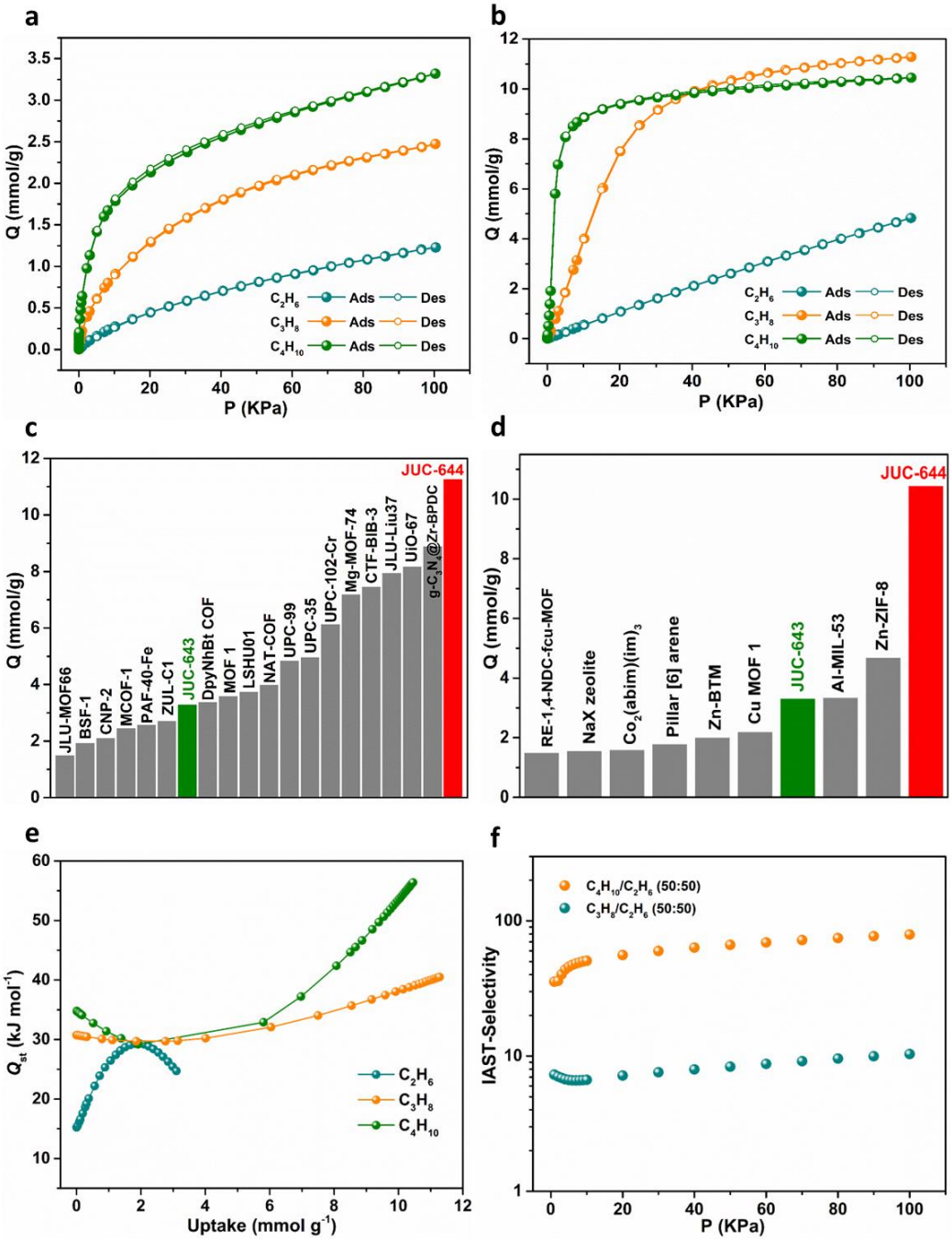

Figure 3. Adsorption and separation towards various light hydrocarbon molecules. a,b, C_2H_6, C_3H_8, and *n*-C_4H_{10} adsorption isotherms at 298 K for JUC-643 (a) and JUC-644 (b). **c,d,** Comparison of adsorption capacities of representative materials for C_3H_8 (c) and *n*-C_4H_{10} (d) at 298 K and 100 Kpa. **e,** Q_{st} of C_2H_6, C_3H_8, and *n*-C_4H_{10} in JUC-644. **f,** IAST selectivity of JUC-644 towards equimolar *n*-C_4H_{10}/C_2H_6 and C_3H_8/C_2H_6 at 298 K.

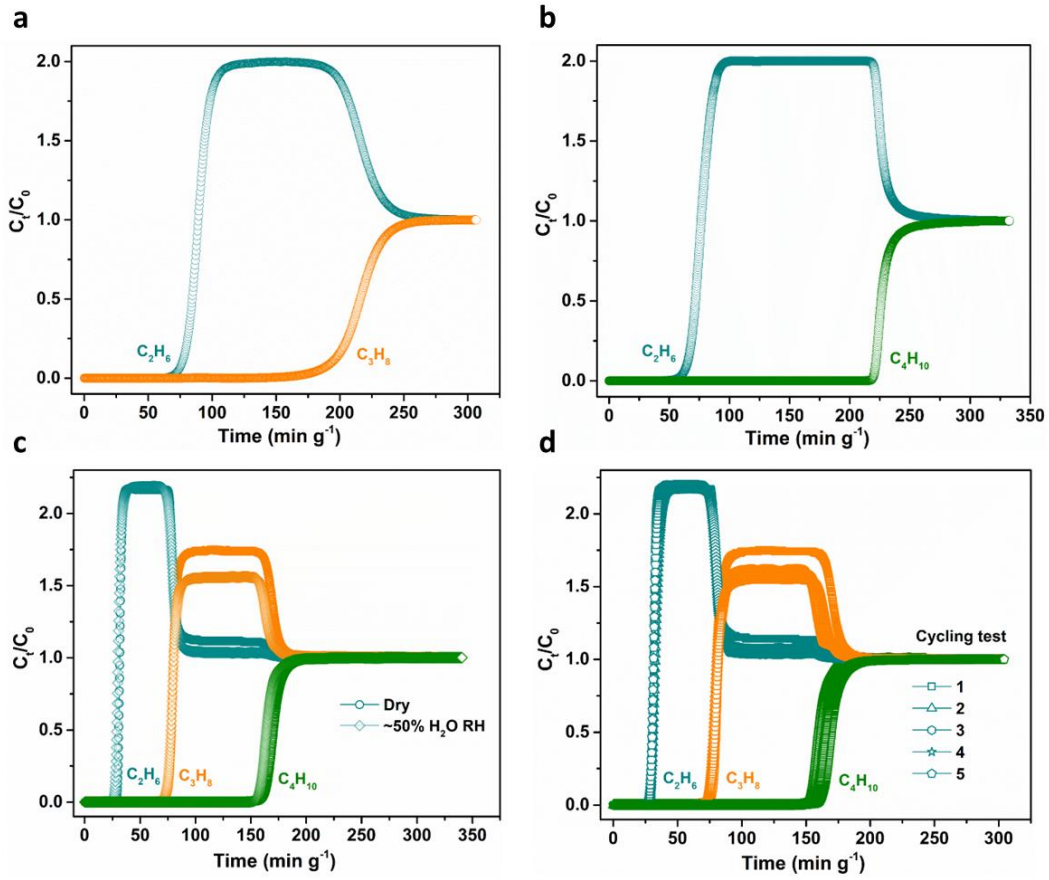

Figure 4. Breakthrough experiments for JUC-644. a,b, The column breakthrough curves for C_2H_6/C_3H_8 (a) and C_2H_6/n-C_4H_{10} (b) mixture (50:50, v/v, Tfr: 2.0 mL min^{-1}) at 298 K. **c,** The column breakthrough curves for dry and moist $C_2H_6/C_3H_8/n$-C_4H_{10} mixture (46:34:20, v/v/v, Tfr: 5.0 mL min^{-1}) at 298 K. **d,** Cycling breakthrough test of $C_2H_6/C_3H_8/n$-C_4H_{10} mixture (46:34:20, v/v/v, Tfr: 5.0 mL/min) at 298 K.

TOC